JETIR.ORG

ISSN: 2349-5162 | ESTD Year : 2014 | Monthly Issue



JOURNAL OF EMERGING TECHNOLOGIES AND INNOVATIVE RESEARCH (JETIR)

An International Scholarly Open Access, Peer-reviewed, Refereed Journal

High-Resolution dynamic modeling over complex terrains of Garhwal Himalaya during winter and pre-monsoon period

Tanmay Dhar¹, Mario M. Miglietta², and Bhupendra S. Rawat¹

- 1 Department of Physics, Uttaranchal University, Dehradun 248007, India
- National Research Council of Italy—Institute of Atmospheric Sciences and Climate (CNR-ISAC), 35127 Padua, Italy

Abstract

The Himalayan climate system is highly susceptible to global and local climate change, and there is ongoing concern about current and potential climate change impacts. In this study, the ERA-Interim dataset (January to May) over the Garhwal Himalayas has been downscaled using the high-resolution (6 km) WRF model and several sensitivity studies have been carried out using microphysics schemes. The downscaled precipitation pattern has sharp features unlike that of ERA-Interim. The WRF model simulated precipitation from various sensitivity experiments has been compared. It is found that there is a shift in the location of maximum precipitation zone in Morrison and Thompson schemes as compared to WSM6 during winter.

Introduction

The inhomogeneous terrain and high altitude of the Himalayas has restricted observational data of the climate system in the region. Therefore, detailed climate of Himalayas is still unknown. Moreover, the western Himalayan region has sharp orography gradient, therefore, the global reanalysis data are too coarse to represent the detailed hydroclimate over the region. As a result, in order to have a high resolution dataset for the region, it is necessary to employ dynamic downscaling method. In this study, the ERA-Interim dataset (January to May) over the western Himalayas has been downscaled using the high-resolution (6 km) WRF model and several sensitivity studies have been carried out using microphysics schemes. The downscaled precipitation pattern has sharp features unlike that of ERA-Interim. The WRF model simulated precipitations from various sensitivity experiments have been compared. It is found that there is a shift in the location of maximum precipitation zone in Morrison and Thompson schemes as compared to WSM6 during winter.

The WSM6 scheme has maximum precipitation more upwind as compared to other schemes as the WSM6 favours precipitation on the slopes of the terrain whereas the Morrison and Thompson schemes produce more snow on the mountain top. This study emphasizes that a correct representation of the microphysical processes in the models is crucial for long-term

climate simulations as these microphysical schemes are responsible for partitioning atmospheric water into vapor, cloud liquid water, cloud ice etc. leading either to solid or liquid precipitation. One of the limiting factor of such studies is the lack of observational data over the Himalayan region to carry out proper verification studies.

The study area

The study area, Garhwal Himalaya is located from 30° N to 31° N latitude and 70° E to 78° E longitudes and comprises an area of 32450 km² (Figure 1). Garhwal Himalaya region is located in Indian Himalayan monsoonal subcontinent and mainly three seasons are present in a year, i.e.warm summer (March to June), humid warm summer (July to June), winter season (November to February). The climatic conditions of the Garhwal Himalayan region vary from the tropical to glacial cover zone. On the basis of temperature, precipitation and altitude, Garhwal Himalaya can be divided into seven different climatic zones from south to north: tropical (< 300 m), subtropical (301-800 m), warm temperate (801-1600 m), cool temperate (1601-2400 m), cold temperate (2401-3200 m), sub-alpine (3201-4000), and glacial cover (> 4000 m) (Kaushik, 1962).

The elevation ranges from 474m (Devaprayag) to 3892m (Gomukh glacier, CWC, 2020). Total number of glaciers identified in Ganga basin is 968 with the glacier covered area coming to about 2,850 km², which is less than 8% of the total basin area. Largest number of glaciers- totaling 407- has been identified in the Alaknanda basin that occupies 1,230 km², which accounts for almost 11% of total basin area (Glacier Atlas of India, GSI, 2017). The land under agriculture is 644.22 km², which is 5.9 percent of the total geographical area while only 64.8 km² (0.6%) land is under the horticultural crops (Sati VP, 2008). Around 60% of the basin is under the agrarian activity (principle crop assortments that incorporate wheat, maize, rice, sugarcane, bajra and potato), while 20% is roofed by backwoods, generally inside the higher mountains; roughly 2% in the mountain peaks is permanently covered with the snow. The annual normal precipitation inside this basin ranges between 550 and 2500 millimeter (Shukla et al., 2014), and a significant part of the precipitation is contributed by the south-westerly monsoon that prevails from July to late September. The geographical location and elective subtleties of the study region of Bhagirathi-Alakananda basin are given in Figure 1.

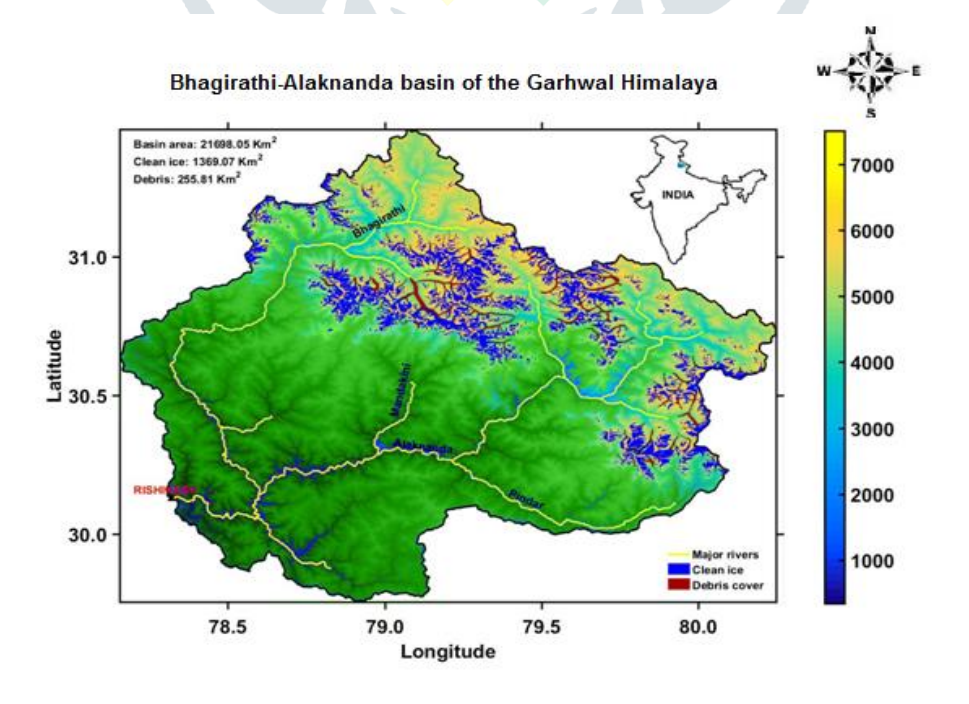


Fig. 1. Elevation of the Garhwal Himalyas

Data

Six hourly high resolution $(0.75^{\circ} \times 0.75^{\circ})$ European Centre for Medium Range Weather Forecast (ECMWF) Reanalysis-Interim (ERA-I) data (Dee et al. 2011) have been used as initial and boundary conditions of the WRF model as well as for model diagnostics. The ERA-I data used in the present study are from January 01, 2018 to June 01, 2018, covering winter and spring periods in the western Himalayan region. This study also utilizes gridded temperature data $(1^{\circ} \times 1^{\circ})$ from IMD (Srivastava et al. 2009) over the Indian region.

WRF Model Configuration

The model used for the present study is the WRF model version 3.7.1 (Skamaraock et al. 2005). The microphysics scheme of the model controls the formation of cloud droplets and ice crystals, their growth and fall down as precipitation. Out of many microphysics schemes available with the WRF model, four schemes have been used in the present study. These are WSM6-class scheme (Hong and Lim 2006), WSM3-class scheme (Hong et al. 2004), Morrison 2-moment scheme (Hong et al. 2004) and Thompson 6-class microphysics scheme with graupel (Thompson et al. 2008). WSM 3-class scheme deals with ice water content and rain/snow. The WSM-6 class microphysics scheme involves the development of graupel. Similar to WSM-6 class scheme, Morrison 2-moment scheme involves the development of graupel in generation of precipitation. In this scheme number concentrations are also predicted for ice, snow, rain and graupel. Thompson scheme deals with mixed phase processes similar to the WSM6 and Morrison schemes. This scheme explicitly predicts the mixing ratios of cloud water, rain, cloud ice, snow, and graupel.

This scheme has the double-moment cloud ice variable and predicts the number concentration of cloud ice. The cloud droplet size distribution assumed in the scheme has a variable gamma shape distribution that shifts according to the assumed droplet number concentration. It may be noted that the WSM3 is a simple ice scheme and does not support mixed-phase processes like the other schemes mentioned above. However, the simulations with WSM3 scheme were included in the present study for the sake of completeness.

All the experiments in the present study used the unified NOAH land-surface model (Chen and Dudhia 2001) with 4-layer soil, and Yonsei University (YSU) planetary boundary layer (PBL) parameterization schemes (Hong and Pan 1996). The Grell-Devenyi convection scheme (Grell and Devenyi 2002) has been used in the present work, in which the convective trigger function is based on grid-resolved vertical velocity. Grell-Devenyi (GD) scheme is formulated as a multi-closure (16 mass flux closure) and it considers ensemble average of more than 100 types of clouds.

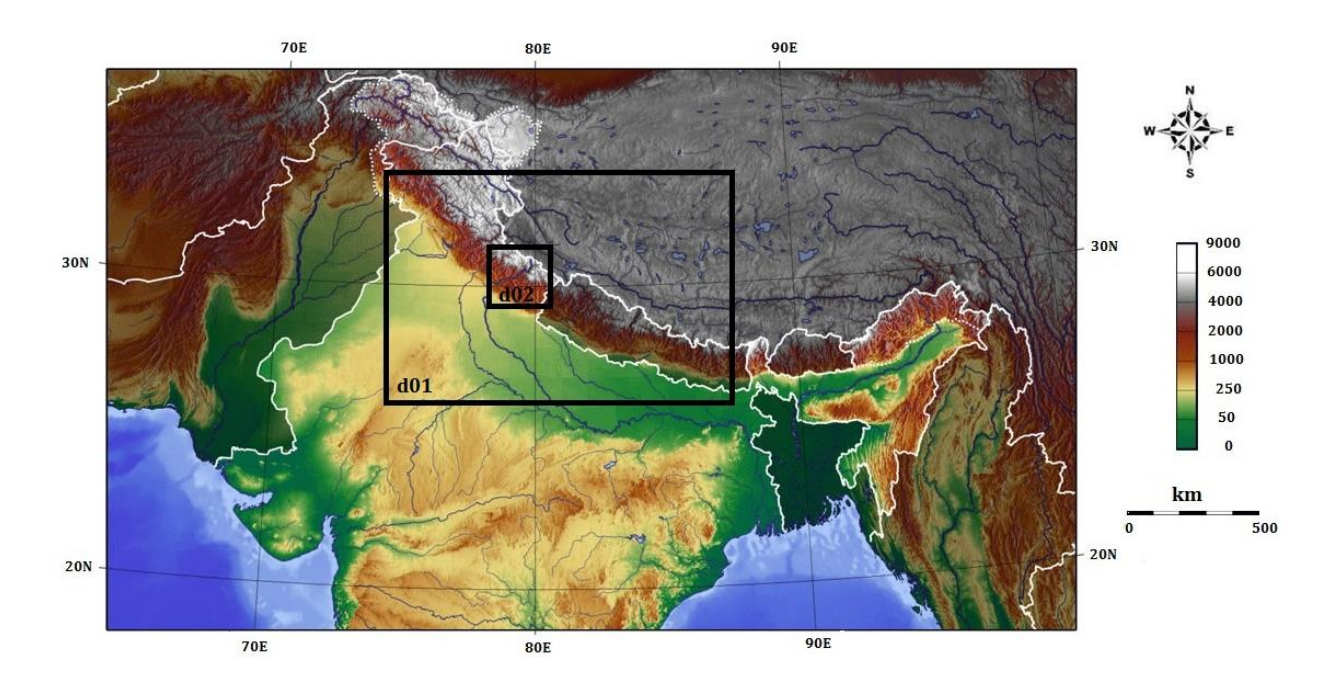


Fig. 2. Model domain

Design of Experiments

Four sensitivity experiments have been carried out using different microphysics while keeping the other scheme the same. The experiments are

(i) CNTL: uses WSM6 scheme

(ii) WSM3: uses WSM3 scheme

(iii) Morrison: uses Morrison scheme

(iv) Thompson: uses Thompson scheme

In the present study, two nested domains of grid spacing of 18 and 6 Km as shown in Fig.1 have been used. For every experiment, the WRF model has been run using initial conditions of 00 UTC of 1 January 2018. All the runs were made till June 01 2018.

CNTL Simulation

Large scale circulation, precipitation patterns including hydroclimate features are first analysed for the bigger domain i.e. Domain-1. The simulations are compared with ERA-I data for mean of January and February (JF) and March, April and May (MAM). Figure 3shows the mean precipitation from WRF model (CNTL) simulations and ERA-I for the Domain-1. During January and February precipitation occurs mostly over western part of the Himalaya as seen in ERA-I (Fig. 3c). There is a northwest-southeast oriented precipitation patch extending upto lower valleys of Uttarakhand. It is noticed that while the precipitation pattern remains the same in MAM as in JF, mean precipitation in MAM is less than that in JF (Fig. 3d). The precipitation patch extends more to the east in MAM as seen in Tiwari et al. (2016) including snowfall that continues in March and April. Precipitation from gridded observed data from IMD has also been examined over the Indian part of the domain (not shown). It is seen from the IMD and reanalysis (ERA-I) datasets that precipitation is mostly received over the western parts of the Himalaya and the precipitation band is oriented south-eastwards towards Uttarakhand with reduced

magnitude. Some amount of precipitation is received over the slope of mountains in Uttarakhand. The model simulated (CNTL) precipitation for JF and MAM are shown in Fig. 1a, b respectively. It is seen that the high-resolution model simulations have sharp features in precipitation in JF as well as in MAM. The ERA-I precipitation is from a coarse resolution model as compared to the WRF model (18 km resolution for Domain-1). In MAM, the model simulates less precipitation as compared to reanalysis data (Fig. 1b). Therefore, it is found that spatial distribution of precipitation over western Himalayas in the WRF model CNTL simulation is similar to the reanalysis products in JF and MAM. Therefore, this model product can be used for further study for the region.

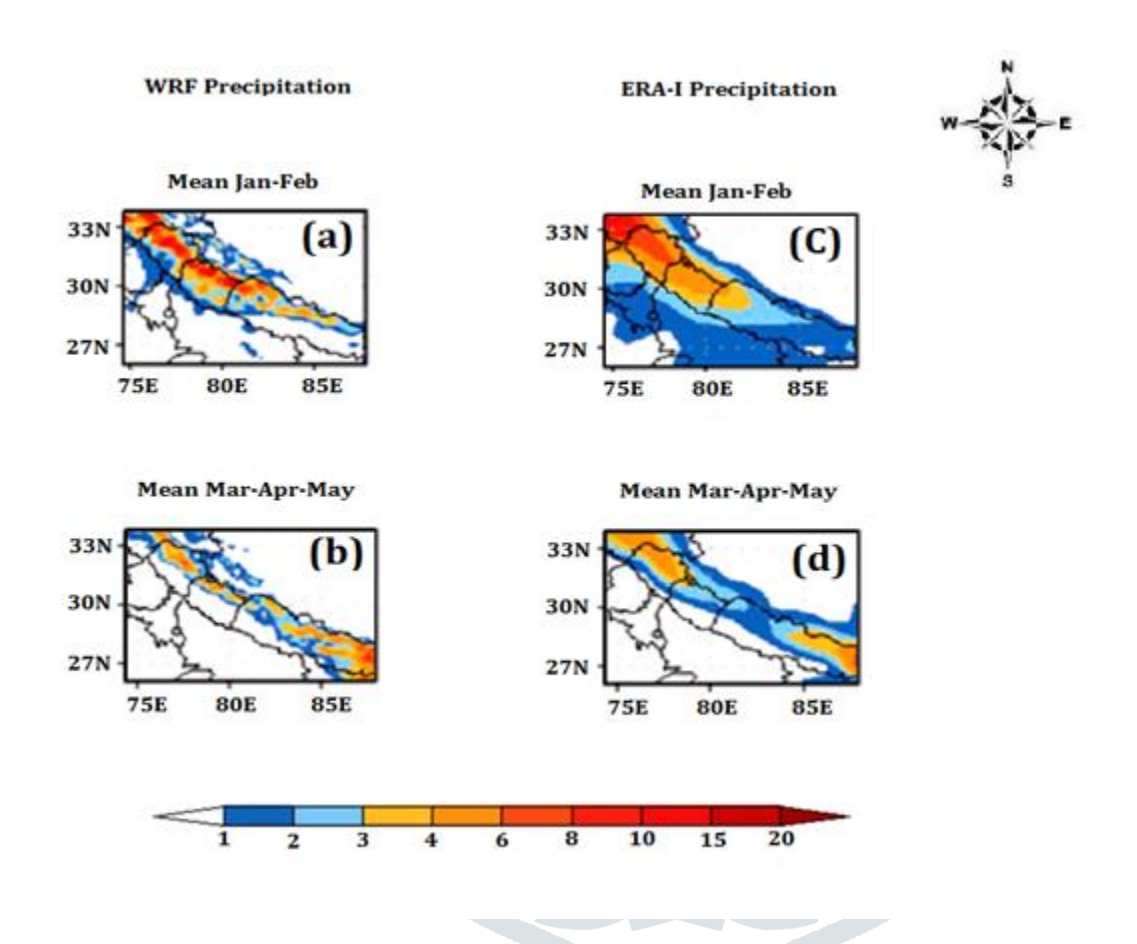


Fig. 3 Mean WRF model (CNTL) simulated precipitation (mm/day) for 2018 (a) January and February (JF); (b) March to May (MAM);). Mean of ERA-I total precipitation (mm/day) for (c) JF; (d) MAM for the same year

The mean winds at 500 hPa for JF and MAM have been examined from reanalysis and WRF model CNTL simulation to establish the consistencies between circulation and precipitation. During winter and spring seasons (JF and MAM), westerly flow dominates the study region and a large number of cyclonic systems (western disturbances) travel across the Himalayan region from west to east. In ERA-I, in JF and MAM a trough is seen in the westerlies around 70°E–80°E and 30°N to 36°N (Fig. 3a, b). The westerly trough is oriented northwest-southeastward. In the model simulations (Fig. 3c, d), all the essential features of the circulation are seen indicating that the model is able to simulate consistent circulation and precipitation over the Domain-1 of the present study.

In order to further downscale the ERA-I data to a smaller domain, the WRF model was configured for the domain-2 as shown in Fig. 1. The horizontal resolution of the model for this nested domain is set at 6 km as compared to 18 km set for domain-1.

All other dynamics and physics options were set the same as the runs for domain-1. Fig. 5 shows the mean of accumulated snow water equivalent (SWE, mm) simulated using WRF model (CNTL run) at the end of February 2018.

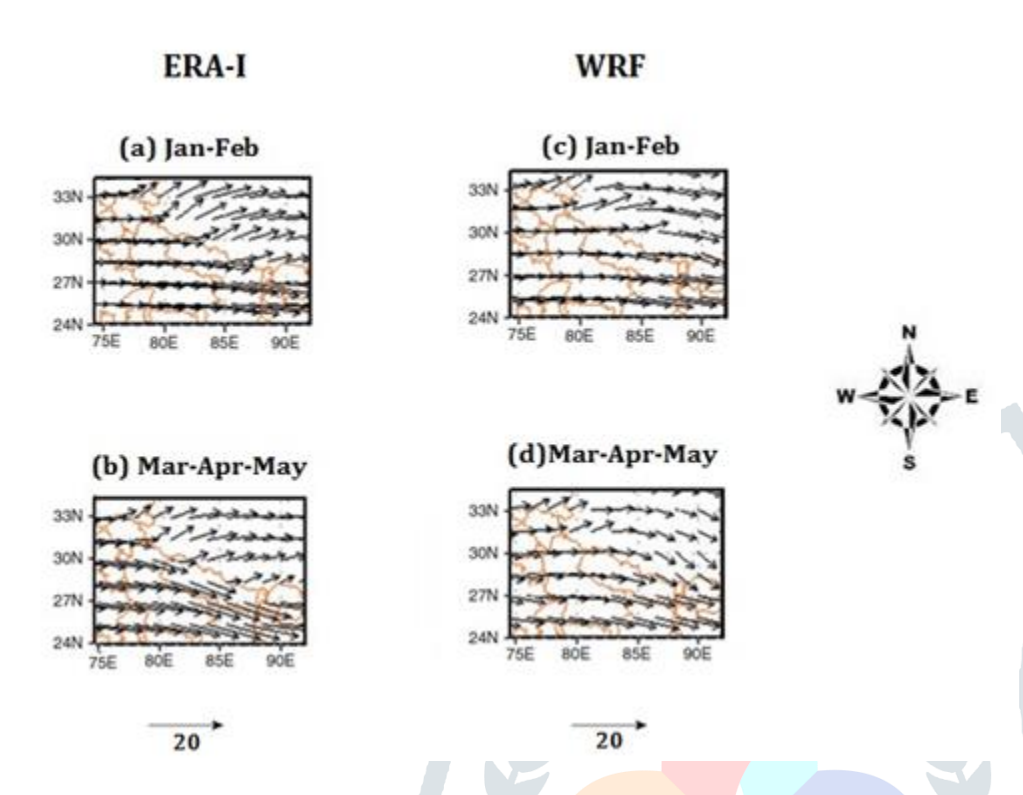


Fig. 4 Mean ERA-I winds (m/s) at 500 hPa for (a) January and February (JF); (b) March, April and May (MAM) for 2018. Mean of WRF model (CNTL) winds (m/s) at 500 hPa for (c) JF; (d) MAM for the same year

SWE describes the amount of water stored within the snow-pack that would be available upon melting and is a major driver of local snowmelt release and hydrological cycles (Derksen et al. 1998). The availability of spatially and temporally extensive SWE data enables a better understanding of space-time trends in snow cover. In situ observations of SWE are made by measuring the snow depth and its density. Observations of microwave sensors are also used to estimate SWE magnitude in large-scale. Tiwari et al. (2016) have examined the large-scale characteristics of SWE using satellite remote sensing data over the western Himalayan region.

In the WRF model, precipitation amount is partitioned into liquid precipitation (rainfall) and solid precipitation (snowfall). Accumulation and ablation of the snowfall occurs based on surface temperature and other meteorological conditions. The model then provides an estimate of accumulated SWE. In the WRF model simulations in the present study, the SWE pattern is characterized by a northwest-southeast band across the Alaknanda basin. In the Domain-2 region (Alaknanda basin), maximum snowfall occurs in March and April. Figure 5c shows the difference of SWE (mm) between the end of May and the end of February 2018. The SWE accumulated on the surface in model simulations at the end of May is more than about 400 mm over most parts of the Alaknanda basin. The zone of Alaknanda basin where maximum snowfall and accumulation occurs is the major catchment area of the Alaknanda river. This area has maximum elevation (> 6000 m) and the Spiti river originating from this area contributes with most of the snowmelt water to Alaknanda River. The accumulated snow at the end of May becomes available for snowmelt runoff in the months of June, July and August.

Sensitivity Studies

A set of sensitivity experiments were carried out using various cloud microphysics schemes in the WRF model and the precipitation simulations over the western Himalayas from these experiments were compared among each other. A composite analysis was made by considering the peak precipitation period during winter (12 days in February 2018) over a part of Bhagirathi-Alaknanda basin and adjoining areas. Figure 6- shows total precipitation from CNTL experiment for the study period. It is seen that the higher elevation regions receive >20 mm/day of precipitation. In contrast, the plain regions in the Bhagirathi-Alaknanda basin get about 5 mm/day. On the slope of higher elevation areas of that basin, it is seen that WSM6 produces more precipitation than other microphysics schemes (Fig. 6b, c). Moreover, the WSM6 scheme has more precipitation than the Morrison scheme over the SE-to-NW precipitation band. Very minor difference (between 1 and 2 mm/day) of precipitation is found between WSM6 and WSM3 schemes (Fig. 6d). Differences in non-convective precipitation in WRF model simulations comefrom the differences in the treatment of phase change of water in the cloud microphysics schemes. Accumulated solid precipitation (snow) and liquid precipitation (rain) obtained from the composite analysis of the study period in February 2018 are shown respectively in Fig.7a, b. It may be noted that during this 12-day period, >500 mm of snowfall was simulated over the higher reaches of the Bhagirathi-Alaknanda basin. Rainfall occurred mostly over the plain areas and lower reaches (Fig.7b). The differences in total solid and liquid precipitation between CNTL and Morrison scheme are shown in Fig.7c, d respectively.

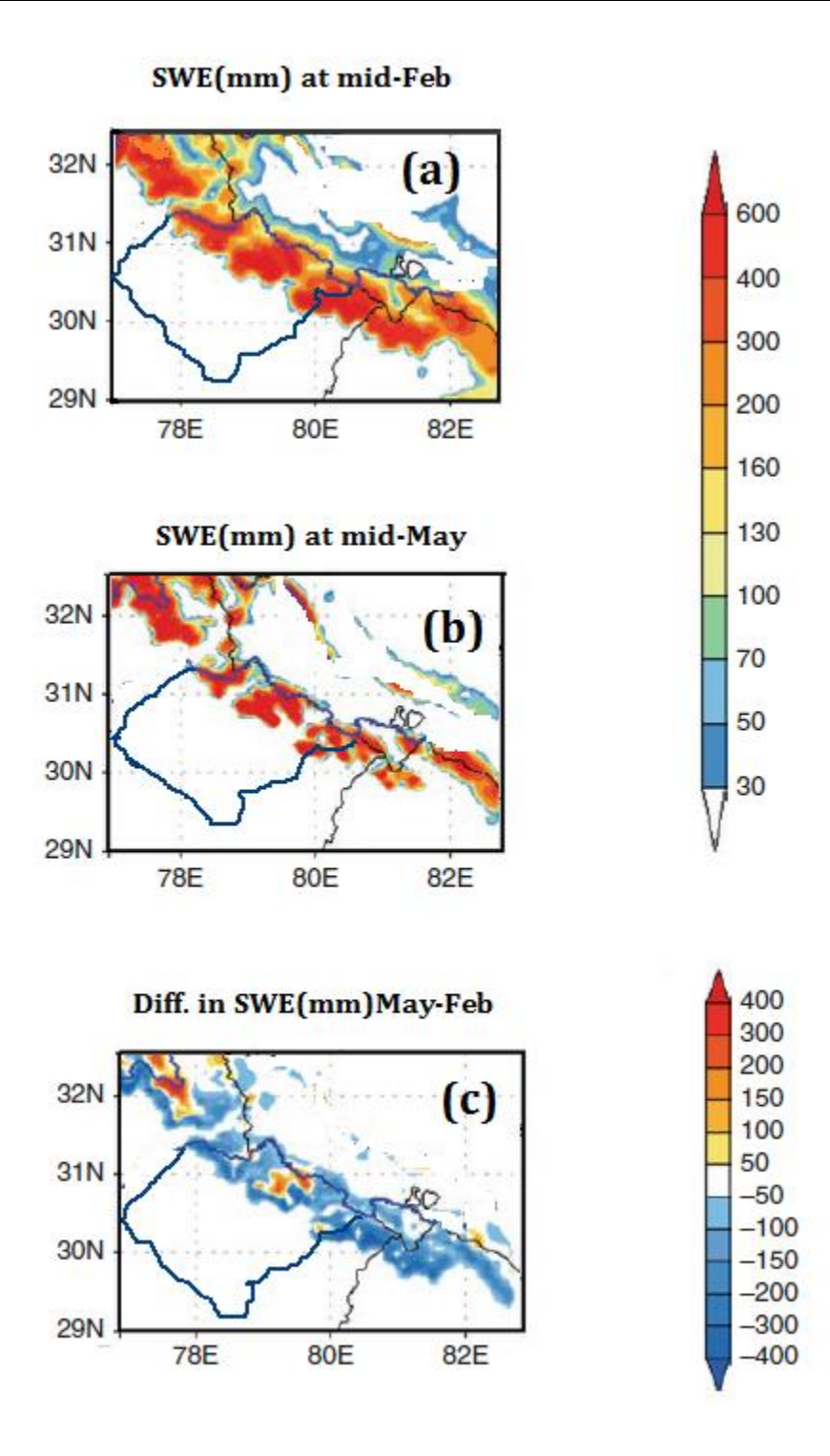


Fig. 5 WRF model (CNTL) simulated snow water equivalent (SWE, mm) accumulation (**a**) at the end of February 2018; (**b**) at the end of May, and (c) difference between SWE (mm) at the end of May and end of February 2018. From the difference plot, it can be seen that the WSM6 (CNTL) scheme simulates more snowfall (> 100 mm/day) than Morrison in the northern part of the domain. However, the Morrison scheme simulates about 100 mm more rain over western and northern region than that in the WSM6 scheme. The differences are similar between CNTL and Thompson scheme, as seen in Fig.7e, f as the Thompson scheme also simulates more snow on the mountain top than CNTL. No large differences are seen between simulated snow or liquid rainfall in WSM3 and CNTL simulations (Fig.7g, h).

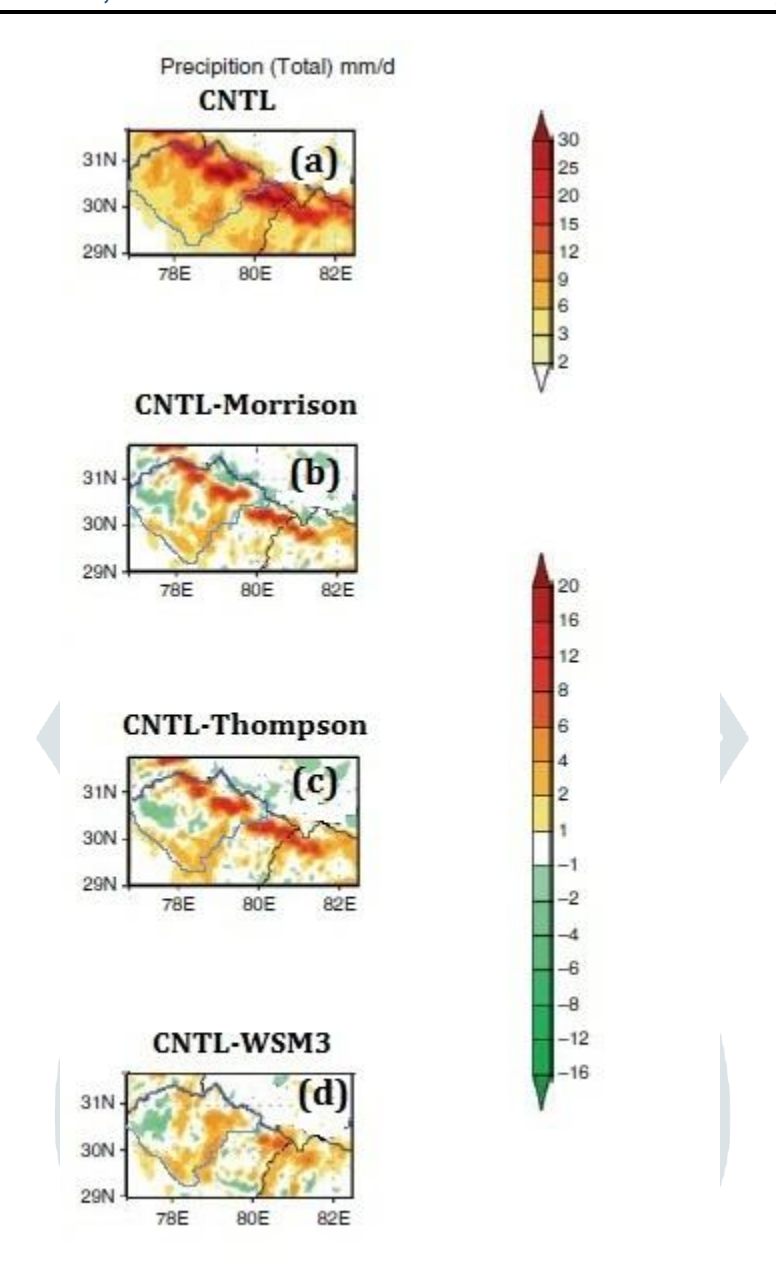


Fig. 6 Composite analysis of total precipitation (mm/day) for excess precipitation days in February 2018 for (a) total precipitation in CNTL; difference in precipitation (mm/day) between CNTL and Morrison; difference between CNTL and Thompson and (d) difference between CNTL and WSM3 experiments.

It may be noted here that in the double moment schemes (e.g. Morrison scheme) particle types vary as a function of the time and the ice mixing ratio is diagnosed separately. As a result of additional moment computation, the double moment scheme (Morrison scheme here) has greater flexibility in representing size distributions impacting simulation of ice, snow, graupels or hail in the present study. In the WRF model simulations, the hydrometeors are separated into non-precipitating particles and precipitating particles.

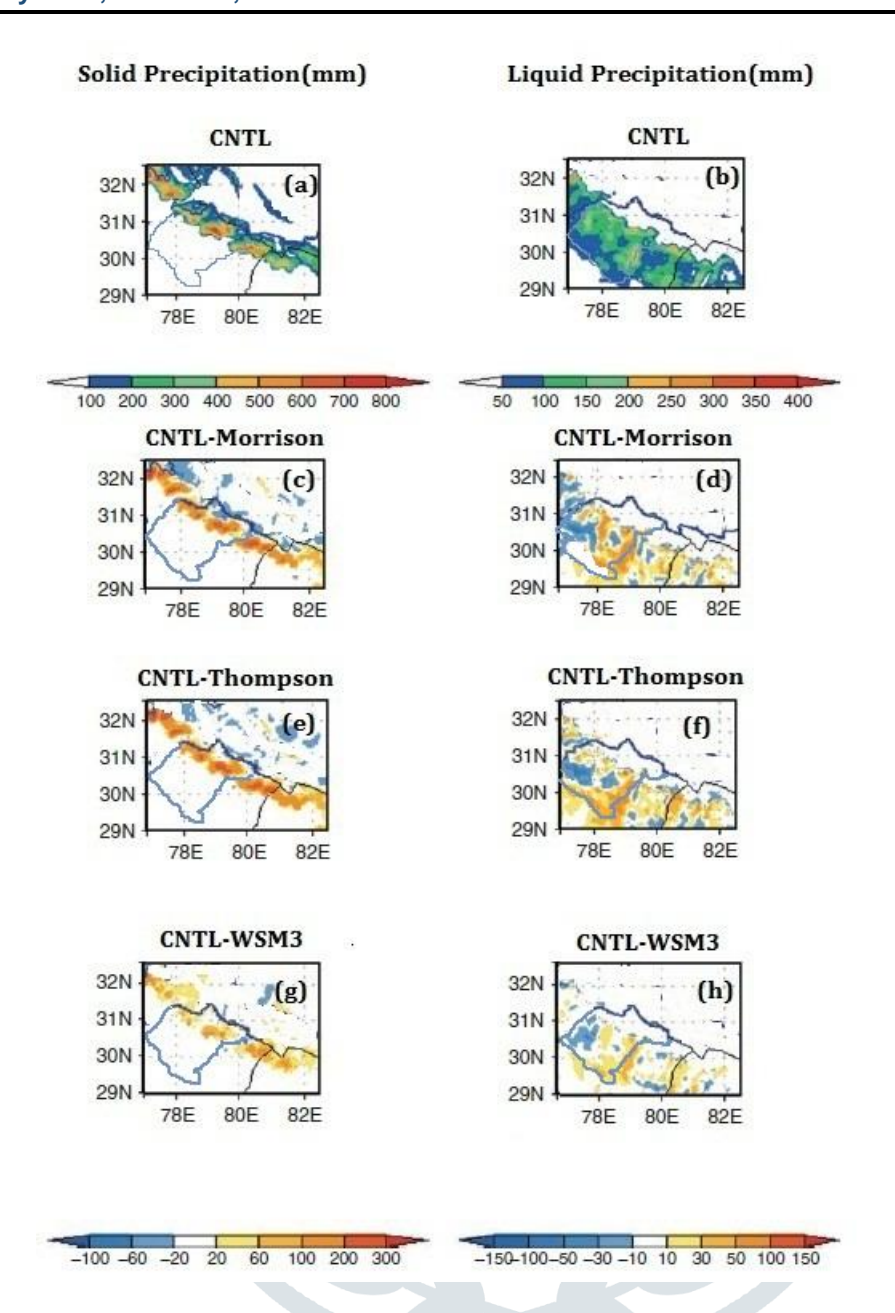


Fig.7 Composite analysis of total solid (snowfall) and liquid (rainfall) precipitation (mm/day) for excess precipitation days in February 2018 for (a) total solid precipitation in CNTL; (b) total liquid precipitation in CNTL; (c) and (d) difference in solid and liquid precipitation (mm/day) between CNTL and Morrison respectively; (e) and (f) difference between CNTL and Thompson; (g) and (h) difference between CNTL and WSM3 experiments.

The mass mixing ratios of cloud and ice (in g/kg) are referred to as QCLOUD and QICE respectively in the present study. The mass mixing ratios of precipitating particles such as rain, snow and graupels are referred to as QRAIN, QSNOW and QGRAUP respectively. Spatial pattern of QSNOW at 500 hPa from CNTL simulation and its difference from the Morrison scheme are depicted in Fig.8a, b respectively. High values of QSNOW (> 12 g/kg) are seen over the region of maximum precipitation. The orientation of QSNOW band is the same as the precipitation band seen earlier. QSNOW has noticeable magnitude between 700 hPa and 300 hPa (not shown). Difference between single moment scheme (WSM6) and double moment scheme (Morrison) indicates that the WSM6 scheme simulates less snow (about 3–4 g/kg) over the peak mountainous region as compared to Morrison, which has more QSNOW downwind. Similar to QSNOW, QICE also forms only above 700 hPa with a

maximum (3–4 g/kg) at about 400 hPa. Figure 8c, d has the plots of QICE at 500 hPa in the study domain from CNTL and its difference between the Morrison scheme.

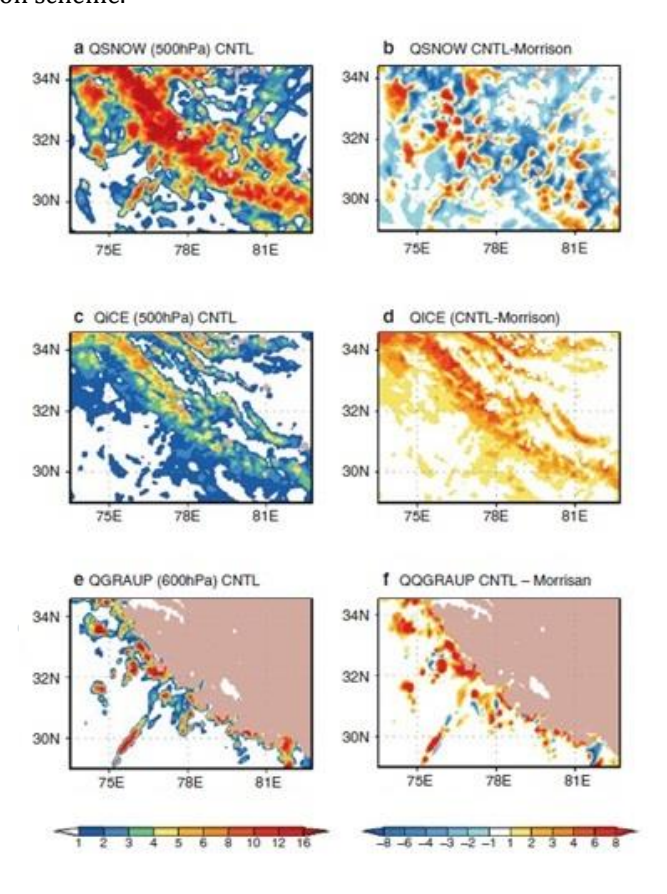


Fig.8 Spatial pattern of hydrometeors in CNTL simulation and their differences between the simulations with the Morrison scheme. (a) QSNOW (g/kg) at 500 hPa; (c) QICE (g/kg) at 500 hPa and (e) QGRAUP (g/kg) at 600 hPa from CNTL simulations. Differences between CNTL and Morrison scheme (b) QSNOW; (d) QICE and (f) QGRAUP

Conclusion

The single moment scheme (WSM6) simulates a larger amount of ice particles at this altitude than the double moment Morrison scheme. Graupel particle (QGRAUPEL) forms only on the windward side of the high mountain at 600 hPa with a maximum of about 6–8 g/kg in CNTL simulations (Fig.8e). It is also seen that in WSM6 scheme, preferred locations of snow and graupel formation is on the upwind side on the mountain slope with the Morrison scheme simulating less graupel. The WSM6 (CNTL) has more rain over the narrow zone of sharply rising orography. However, the Morrison scheme has more precipitation downstream at higher elevations.

References

Chen, F., and J. Dudhia (2001), Coupling an advanced land surface-hydrology model with the Penn State-NCAR MM5 modeling system. Part I: Model implementation and sensitivity, *Mon. Weather Rev.*, **129**, 569–585, doi:10.1175/1520-0493(2001)129<0569:CAALSH>2.0.CO;2

Dee, D. P., Uppala, S. M., Simmons, A. J., Berrisford, P., Poli, P., Kobayashi, S., Andrae, U., Balmaseda, M. A., Balsamo, G., Bauer, P., Bechtold, P., Beljaars, A. C. M., van de Berg, L., Bidlot J., Bormann, N., Delsol, C., Dragani, R., Fuentes, M., Geer, A. J., Haimberger, L., Healy, S. B., Hersbach, H., Hólm, E. V., Isaksen, L., Kållberg, P., Köhler, M., Matricardi, M., McNally, A. P., Monge-Sanz, B. M., Morcrette, J.-J., Park, B.-K., Peubey, C., de Rosnay, P., Tavolato, C., Thépaut, J.-N., and Vitart, F.(2011), The ERA-Interim

reanalysis: configuration and performance of the data assimilation system, Q. J. Roy. Meteorol. Soc., 137, 553-597, https://doi.org/10.1002/qj.828

Derksen, C., LeDrew, E. and Goodison, B. (1998), SSM/I derived snow-water equivalent data: the potential for investigating linkages between snow-cover and atmospheric circulation. Atmosphere-Ocean 36, 95-117.

Grell, G. A. and Dévényi, D.(2002), A generalized approach to parameterizing convection combining ensemble and data assimilation techniques, Geophys. Res. Lett., 29, 1693, https://doi.org/10.1029/2002GL015311

Hong, S. Y. and Lim, J. O. J. (2006), The WRF single-moment 6-class microphysics scheme (WSM6), J. Korean Meteorol. Soc., 42, 129–151.

Hong, S-Y., , J. Dudhia, , and S-H.Chen, (2004), A revised approach to ice microphysical processes for the bulk parameterization of clouds and precipitation. *Mon. Wea. Rev.*, **132**, 103–120.

Hong, S-Y., and H-L. Pan, (1996), Nonlocal boundary layer vertical diffusion in a medium-range forecast model. *Mon. Wea. Rev.*, **124**, 2322–2339.

Kaushik, S.D.(1962). Climatic Zones and the Related Socio - economy of the Garhwal Himalaya. Geog. Rev. India, 24 (3-4)

Skamarock, W. C., J. B. Klemp, J. Dudhia, D. O. Gill, D. M. Barker, W. Wang, and J. D. Powers (2005), A description of the advanced research of WRF version 2, *Tech. rep. TN-468+STR*, Natl. Cent. for Atmos. Res., Boulder, Colo.

Srivastava, A.K., Rajeevan, M. and Kshirsagar, S.R (2009), Development of High Resolution Daily Gridded Temperature Data Set (1969-2005) for the Indian Region. Atmos. Sci. Lett. DOI: 10.1002/asl.232.

Thompson G., P. R. Field, R. M. Rasmussen, and W. D. Hall (2008), Explicit forecasts of winter precipitation using an improved bulk microphysics scheme. Part II: Implementation of a new snow parameterization, Mon. Wea. Rev., 136, 5095–5115

Tiwari S, Kar SC, Bhatla R. (2016). Interannual variability of snow water equivalent (SWE) over western Himalayas. *Pure Appl. Geophys.* **173**(4): 1317–1335.